# Modeled Response of Greenland Snowmelt to the Presence of Biomass Burning-Based Absorbing Aerosols in the Atmosphere and Snow

Jamie L. Ward, Mark G. Flanner, Mike Bergin, Jack E. Dibb, Chris M. Polashenski, Amber J. Soja, Jennie L. Thomas

## HAL Id: insu-01799323
## https://insu.hal.science/insu-01799323

Submitted on 12 Aug 2020

# Modeled Response of Greenland Snowmelt to the Presence of Biomass Burning-Based Absorbing Aerosols in the Atmosphere and Snow

**Jamie L. Ward**[1] iD, **Mark G. Flanner**[1] iD, **Mike Bergin**[2] iD, **Jack E. Dibb**[3] iD, **Chris M. Polashenski**[4,5] iD, **Amber J. Soja**[6] iD, and **Jennie L. Thomas**[7] iD

[1]Department of Climate and Space Sciences and Engineering, University of Michigan, Ann Arbor, MI, USA, [2]School of Civil and Environmental Engineering, Duke University Durham, Durham, NC, USA, [3]Earth Systems Research Center, EOS, University of New Hampshire, Durham, NH, USA, [4]CRREL, USACE, Ft. Wainwright, AK, USA, [5]Thayer School of Engineering, Dartmouth College, Hanover, NH, USA, [6]National Institute of Aerospace, NASA Langley Research Center, Hampton, VA, USA, [7]LATMOS, Paris, France

**Abstract** Biomass burning produces smoke aerosols that are emitted into the atmosphere. Some smoke constituents, notably black carbon, are highly effective light-absorbing aerosols (LAA). Emitted LAA can be transported to high-albedo regions like the Greenland Ice Sheet (GrIS) and affect local snowmelt. In the summer, the effects of LAA in Greenland are uncertain. To explore how LAA affect GrIS snowmelt and surface energy flux in the summer, we conduct idealized global climate model simulations with perturbed aerosol amounts and properties in the GrIS snow and overlying atmosphere. The in-snow and atmospheric aerosol burdens we select range from background values measured on the GrIS to unrealistically high values. This helps us explore the linearity of snowmelt response and to achieve high signal-to-noise ratios. With LAA operating only in the atmosphere, we find no significant change in snowmelt due to the competing effects of surface dimming and tropospheric warming. Regardless of atmospheric LAA presence, in-snow black carbon-equivalent mixing ratios greater than ~60 ng/g produce statistically significant snowmelt increases over much of the GrIS. We find that net surface energy flux changes correspond well to snowmelt changes for all cases. The dominant component of surface energy flux change is solar energy flux, but sensible and longwave energy fluxes respond to temperature changes. Atmospheric LAA dampen the magnitude of solar radiation absorbed by in-snow LAA when both varieties are simulated. In general, the significant melt and surface energy flux changes we simulate occur with LAA quantities that have never been recorded in Greenland.

## 1. Introduction

One of the most important influences on Earth's climate system is the production, transport, and deposition of aerosols. These tiny solid or liquid particles can influence incoming solar radiation (insolation) directly through scattering and absorption, or indirectly by serving as cloud condensation nuclei (CCN) and generating clouds that reduce insolation at the surface. Although most aerosol species predominantly scatter insolation and cool the surface, some species strongly absorb insolation. Of these light-absorbing aerosols (LAA), black carbon (BC) has the highest absorptivity. BC is produced by the incomplete combustion of biomass, biofuels, or fossil fuels and tends to be emitted along with less absorptive species (Bond et al., 2013; Chung & Seinfeld, 2002; Hansen & Nazarenko, 2004; Koch et al., 2009; Ocko et al., 2012). The radiative and meteorological effects of BC are difficult to assess because the processes of emission, transport, and deposition distribute it heterogeneously across the globe (Liu et al., 2012; Ramanathan & Carmichael, 2008). As BC emissions continue to evolve in the future, regional atmospheric temperature and precipitation patterns could change in response (Menon et al., 2002).

BC is especially important for the climate system and local energy budget because it efficiently absorbs radiation in the visible wavelengths (0.4–0.7 μm), which make up the largest portion of energy emitted by the Sun (Bond et al., 2013; Koch et al., 2009). Through the direct aerosol effect, BC presence can lead to localized warming in the atmosphere or on the surface, affecting atmospheric stability, cloud formation, and sensible and latent heat fluxes at the surface (Ban-Weiss et al., 2011; Flanner, 2013; Ramanathan & Carmichael, 2008). Indirect effects of LAA that result from cloud formation can also significantly impact these processes. Unlike greenhouse gases, which warm the surface regardless of height in the atmosphere, the altitude of BC is

important when considering its net energy impact at the surface. Regardless of its position, BC in the atmosphere leads to positive top-of-atmosphere forcing on a global scale due to its high absorptivity. Direct surface radiative forcing from BC in the atmosphere is negative because it reduces surface insolation. In an idealized modeling framework focusing on the Arctic, Flanner (2013) determined that the altitude of BC is an important factor for surface temperature response. Flanner's (2013) results indicate that BC suspended in the lowest portion of the atmosphere leads to surface warming. This surface warming decreases as BC is suspended at higher altitudes, eventually transitioning to surface cooling with BC suspended above roughly 450 hPa (Flanner, 2013). Haywood and Ramaswamy (1998), Ramanathan and Carmichael (2008), and Ban-Weiss et al. (2011) also note the importance of vertical aerosol distribution on surface processes.

Several processes and feedbacks impact the net effect of atmospheric aerosols. Localized atmospheric warming resulting from suspended BC can lead to cloud burn-off (i.e., cloud droplet dissipation). In this process, local air becomes unsaturated as a result of increasing air temperatures and cloud droplets evaporate (Ban-Weiss et al., 2011; Flanner, 2013; Ramanathan & Carmichael, 2008; Sand et al., 2013; Wang, 2004). BC-based warming can also lead to changes in the vertical lapse rate of the atmosphere and local stability, depending on BC altitude. Within the aerosol layer, diabatic warming associated with the aerosols leads to local destabilization of the atmosphere and can result in cloud formation (Ban-Weiss et al., 2011; Wang, 2004). High-altitude BC often leads to atmospheric stabilization and inhibits convective low cloud formation as a result of warming the air aloft and cooling the surface (Ban-Weiss et al., 2011; Flanner, 2013). Decreased atmospheric stability results from the presence of deposited BC. Deposited BC leads to surface warming, resulting in steepening of the lower tropospheric adiabatic lapse rate and atmospheric destabilization (Ban-Weiss et al., 2011; Flanner, 2013).

LAA are especially influential on the climate of snow- and ice-covered polar regions. Flanner et al. (2007) determined that absorptive biomass burning and fossil fuel emissions led to Arctic air warming by $0.50 - 1.61°C$ . This is large relative to the global emission-based warming of $0.10 - 0.15°C$ (Flanner et al., 2007). In-snow impurities like BC and dust also increase surface energy fluxes into the surface through snow-albedo feedback mechanisms. BC and dust darken the snow and enhance solar energy absorption at the surface. As a result of this extra energy, snowmelt and snow aging are enhanced (Hansen & Nazarenko, 2004). In the perennial snow that covers the GrIS, meltwater can cause impurities to percolate downward into the snowpack, though buried impurities can also become reexposed when overlying snow is removed, further reducing surface albedo (Painter et al., 2012). The outsize impact of LAA on high-albedo areas suggests that these aerosols could have a significant impact on the Greenland Ice Sheet (GrIS), a high albedo, perennially snow and ice covered surface, with implications for sea level rise. If the entire GrIS were to melt, projected sea level rise is estimated to be 7.4 m, which could lead to the destruction of populous coastal cities across the globe (Gregory et al., 2004; Hanna et al., 2008). One of the climatic factors that could enhance future GrIS melt is altered presence of LAA in the Greenland region. BC and other LAA are transported to the GrIS through global circulation mechanisms and cyclonic storms. Measurements and simulations indicate that LAA transport to the Greenland region normally begins to increase in March, with concentrations peaking in the summer months before tapering off in autumn (Jiao et al., 2014; Polashenski et al., 2015). However, Greenland currently receives lower concentrations of BC than other Arctic locations (Jiao et al., 2014). As a land mass of perennial snow and ice cover, though, the GrIS is more susceptible to the effects of snow darkening than most other areas of the Arctic.

Biomass burning-based BC emissions contribute roughly 40% of all global BC emissions, which suggests that biomass burning is an important influence on global climate (Ramanathan & Carmichael, 2008). The frequency of sustained, extreme biomass burning depends on regional temperature and precipitation. Higher temperature and lower precipitation conditions are more conducive to larger-scale, uncontrollable fire activity. Boreal climates are warmer and drier now than they have been for much of the past 10,000 years (Kelly et al., 2013). Under future climate scenarios, it is predicted that fire frequency, burned area, severity, and fire season length will increase (Flannigan et al., 2009, 2013; Stocks et al., 1998). There is already evidence of fire-induced change across the circumboreal (Jolly et al., 2015; Soja et al., 2007). In addition to boreal forests, it has been predicted that biomass burning activity in other regions will also increase where fire suppression is not practiced (Marlon et al., 2013). For example, Spracklen et al. (2009) used global climate model-based meteorological output and stepwise regression techniques to test this hypothesis for the western United States. They found that the total land area affected by biomass burning will increase by 54% by the middle of the

21st century as a result of changing regional climate patterns (Spracklen et al., 2009). With increased biomass burning activity, more BC could be emitted and transported to sensitive environments like the GrIS. The resulting BC could lead to greater GrIS snowmelt as a result of surface albedo reduction. We have observed that BC produced from biomass burning can be transported to the GrIS. Recent measurements of elevated GrIS BC have been shown to be coupled with high $NH_4^+$ mixing ratios, suggesting that these BC samples were produced from remote biomass burning events (Keegan et al., 2014; Polashenski et al., 2015). Thomas et al. (2017) confirmed that BC deposited on the GrIS in early August of 2013 originated from biomass burning activity in Quebec and western Canada using a combination of transport modeling, satellite data analysis, and snow pit measurements. Although the quantity of BC deposited from the fire activity cited by Thomas et al. (2017) could have led to significant GrIS albedo reduction, Polashenski et al. (2015) determined that this was not the case because the BC was buried by fresh snow days after its deposition. Given that sunlight intensity decreases in August, this magnitude of BC on the GrIS would have been more effective at reducing surface albedo if it had taken place in late spring or early summer (Polashenski et al., 2015). However, biomass burning is a key and uncertain source of Arctic LAA in the summer.

Although many studies have investigated the direct radiative forcing of BC and other LAA on a global scale (e.g., Ban-Weiss et al., 2011; Bond et al., 1998; Clark et al., 2015; Flanner et al., 2007; Jacobson, 2001, 2004; Wang, 2004) and in the Arctic (e.g., Flanner, 2013; Jiao et al., 2014; Sand et al., 2013; Wang et al., 2011) using various modeling techniques, the relative impacts of biomass burning-based atmospheric and deposited LAA on GrIS snowmelt have yet to be investigated. In this study, we use idealized global climate modeling techniques to examine the relative impacts of atmospheric and deposited LAA on GrIS snowmelt and surface energy fluxes from June through August. First, we describe the methods we use for setting up the model simulations and analyzing the results in section 2. We then demonstrate how different aerosol concentrations and positional combinations lead to varying GrIS snowmelt and surface energy patterns in section 3. Finally, we summarize the results and implications of this research in the conclusion.

## 2. Methods

To explore the extent to which atmospheric and deposited LAA can affect GrIS snowmelt and other climatic conditions in the summer, we conduct four sets of experiments. The "AOD-ONLY" experiment varies atmospheric aerosol burden without any BC or dust in the GrIS snow. Similarly, we explore the effects of changing atmospheric aerosol single-scatter albedo (SSA) in runs with constant atmospheric aerosol burden ("Variable SSA" or "VSSA"). We analyze different SSA values because the ratio of BC to organic carbon (OC) in smoke depends largely on the biomass type being burned (Bond et al., 2013). OC is less absorptive than BC, so more OC in a smoke plume indicates higher SSA (Bond et al., 2013). We examine the climate effects of BC and dust deposited on the GrIS by changing in-snow aerosol mixing ratios and zeroing out all atmospheric aerosols in the "IN-SNOW" runs. Finally, to evaluate the effects of aerosols present simultaneously in the atmosphere and on the GrIS surface, we conduct the "BOTH" runs. Although BOTH more accurately depicts LAA conditions (i.e., high atmospheric LAA are required for high deposited LAA content), we conduct AOD-ONLY, VSSA, and IN-SNOW to isolate the climate impacts of LAA location. For all of these simulations, we use the Community Earth System Model (CESM), version 1.0.3. We apply CESM with a spatial resolution of $1.9° \times 2.5°$ and a time step of 30 min. Although the spatial resolution may seem somewhat coarse, the land surface of Greenland is present in 121 grid cells that we use for our analysis. We run each simulation for 11 model years and analyze monthly model output. To accommodate the time required for atmospheric equilibration, we discard the first year of each model simulation for spin-up purposes. Regardless of the experiment, the aerosol burdens and optical properties we specify at the start of each model run remain constant for the entire simulation. We specifically investigate the climate response during the summer (June, July, and August) because this is when Greenland receives the greatest amount of insolation. During these months, the direct radiative forcing that results from suspended LAA is responsible for air temperature enhancement throughout the troposphere (Screen et al., 2012). Although aged, hydrophilic BC can indirectly affect the propagation of radiation by serving as CCN, we do not address these effects on Greenland's climate in this study.

For each simulation, we couple Community Atmosphere Model 4.0 (CAM4) and Community Land Model 4.0 (CLM4) while prescribing annually repeating present-day climatological sea surface temperatures and sea ice.

While the use of fixed sea surface temperatures does not capture the full climate response to aerosols, we use this setup because less model noise is produced, the model output contains less interannual variability, and less spin-up time is needed, all of which facilitate a more straightforward interpretation of the effects of aerosol loading above and on the GrIS. The SNow, ICe, and Aerosol Radiation model (SNICAR) is a standard component of CLM that we adapt for our experiments to simulate the radiative effects of aerosols in snow on the GrIS. SNICAR is a two-stream, multilayer, multiple-scattering radiative model (e.g., Flanner & Zender, 2005). SNICAR calculates surface albedo and vertical heating in the snowpack using solar zenith angle, ice effective grain size, and BC, OC, and dust mass concentrations (Oleson et al., 2010). Snow grains and impurities are represented as spheres for Mie calculations that are used in the two-stream setup (Oleson et al., 2010). Although SNICAR normally diagnoses impurity mass changes in each snow layer associated with new snowfall and meltwater percolation, we choose to maintain constant mass mixing ratios in each layer for experiments conducted here, ensuring consistency with our imposition of constant aerosol burdens in the atmosphere.

Because the purpose of this study is to isolate the climate effects of LAA above and on the GrIS, we prescribe identical three-dimensional climatological aerosol fields (Lamarque et al., 2010) outside of Greenland in all experiments. We define the Greenland area to span land within latitude and longitude ranges of $60 - 85°N$ and $20 - 60°W$, respectively. Within this region, we manually vary atmospheric and terrestrial aerosol burdens, as well as aerosol SSA. For the atmospheric aerosol simulations, we impose a specific aerosol burden in the lowest five vertical layers of CAM, or approximately the lowest 2 km of the atmosphere overlying the GrIS. All aerosols are zeroed out above the lowest five atmospheric layers in CAM. Although we could perform additional simulations with LAA placed at different altitudes above Greenland, we do not explore the vertical dimension in this study. Flanner (2013) finds that air temperature and net radiation at the surface decrease as the altitude of BC increases. Given the similar setup to their study, we hypothesize that this would also be the case for our AOD-ONLY simulations. It is important to emphasize that the aerosols within this Greenland region are not advected by the model. Instead, aerosol quantities and properties that we define remain constant over all of the Greenland region throughout the entire simulation.

To determine how varying atmospheric LAA burdens affect GrIS snowmelt, we specify aerosol optical depth (AOD), or the opacity associated with the suspended particles, over the entire Greenland region. Functionally, we achieve this by setting the burdens of hydrophobic BC and OC, each of which have unique values of mass extinction cross section and SSA, to the exact quantities that achieve the desired AOD and SSA. We distribute their total burdens evenly among the five lowest atmospheric layers of CAM. Suspended BC and OC burdens are also distributed uniformly across the Greenland region. All other aerosol species are absent from Greenland's atmosphere. We choose AOD as a proxy for aerosol concentration because much of the available atmospheric aerosol data over Greenland are measured in terms of AOD. We examine the climate response to atmospheric aerosols by changing AOD while maintaining constant aerosol SSA in the AOD-ONLY simulations. We note again that the imposed aerosols do not directly affect cloud microphysics. These LAA only affect the propagation of radiation through the atmosphere, which subsequently impacts diabatic heating and bulk thermodynamic processes. The choice of values for the AOD-ONLY cases is based on AOD measurements taken by Strellis et al. (2013) over Summit, Greenland, in the summer of 2011. These measurements were taken using handheld Sun photometers; AOD = 0.09 ± 0.03 (used in case AOD = 0.09) was the average value over the entire summer, and AOD = 0.21 (used in case AOD = 0.21) was the maximum measurement (Strellis et al., 2013). Based on in situ scattering measurements that Strellis et al. (2013) also took over Summit, the average SSA of the suspended aerosols was 0.93 ± 0.03. We incorporate these measurements in our AOD-ONLY runs by imposing constant SSA = 0.93 in every case. We also consult other Arctic-based AOD measurements to establish extreme scenarios of aerosol loading associated with high-impact biomass burning events. Using measurements taken over select Arctic locations during the summer of 2004, Stohl et al. (2006) determined that the average AOD of LAA produced by extensive remote biomass burning activity was 0.50, which we use for our third AOD-ONLY case. For the final two AOD-ONLY cases, we set extremely high AOD values of AOD = 0.75 and AOD = 1.0, which are 50% and 100% larger than the AOD = 0.50 case, respectively. Thomas et al. (2017) showed that for intense fires 550 nm AOD values (Moderate Resolution Imaging Spectroradiometer [MODIS] Aqua) were close to 1 over the source fires in Canada and over Hudson Bay in summer 2013. However, detection of AOD over the Greenland ice sheet during fire events was limited by cloud cover. Although aerosol extinction associated with AOD > 0.50 has not been

**Table 1**
*LAA Model Input for Each Experiment[a]*

| Experiment Rank | AOD-ONLY[b] AOD | BOTH IN-SNOW BC (ng/g) | BOTH IN-SNOW Dust (ng/g) | BOTH IN-SNOW BCE (ng/g) | VSSA[c] SSA |
|---|---|---|---|---|---|
| 1 | 0.09 | 2.6 | 54.8 | 2.7 | 0.90 |
| 2 | 0.21 | 15 | 328 | 15.7 | 0.93 |
| 3 | 0.50 | 58.8 | 1360 | 61.8 | 0.96 |
| 4 | 0.75 | 88.2 | 2040 | 92.8 | -- |
| 5 | 1.00 | 117.6 | 2720 | 123.7 | -- |

[a]AOD, BC and dust mixing ratios (and the associated BCE for each case), and SSA values used in CESM for AOD-ONLY, IN-SNOW, BOTH, and VSSA simulations. [b]SSA = 0.93 for each case. [c]AOD = 0.50 for each case.

measured in the generally pristine Greenland atmosphere, we simulate the unrealistic AOD = 0.75 and AOD = 1.0 cases to achieve high signal-to-noise ratios and more wholly characterize the sensitivity of Greenland's climate to atmospheric LAA. The values of aerosol properties that we use for all of our simulations are shown in Table 1. Given the measured range of SSA values by Strellis et al. (2013), we conduct two additional runs with AOD = 0.50 and varying SSA values (i.e., SSA = 0.90 and SSA = 0.96) in the VSSA experiment to examine how changing SSA affects Greenland's climate (Table 1).

Because aerosols also darken snow surfaces after being deposited, we run a suite of five IN-SNOW simulations to assess the effects of LAA deposited on the GrIS. In these simulations, we vary BC and dust mixing ratios in snowpack based on measured and theoretical values. We include dust in our simulations because dust also contributes to the absorption of sunlight in snow (Painter et al., 2007). Unlike with the AOD-ONLY and VSSA experiments, we represent deposited LAA quantities as mixing ratios because these are the quantities for which we have measurements. Although we specify BC and dust mixing ratios throughout the entire snow column, we note here that it is the presence of LAA only in the top several centimeters of snow that causes most of the sunlight absorption. We simulate BC with a number mean radius of 50 nm using one size bin. We distribute specified dust mixing ratios among the four size bins applied by SNICAR, with lognormal size functions partitioned into each of the bins. The minimum particle sizes of these four bins are 0.01, 1.0, 2.5, and 5.0 $\mu$m, and the corresponding volume fractions for the assumed size distribution are 44.53%, 43.66%, 10.37%, and 1.45%, respectively.

To concisely represent the total amount of LAA in snow, we refer to the combined mixing ratios of BC and dust in this discussion using a black carbon equivalent (BCE) metric with units of ng/g:

$$BCE = [BC] + \sum_{i=1}^{4} \left( \frac{[Dust]_i * MAC_{Dust,i}}{MAC_{BC}} \right). \tag{1}$$

In this equation, $[BC]$ is the mixing ratio of BC, $[Dust]_i$ is the mixing ratio of dust in size bin $i$, and the mass absorption cross sections (MAC) for dust in bin $i$ and BC are $MAC_{Dust,\,i}$ and $MAC_{BC}$, respectively. This metric represents the equivalent BC mixing ratio when we take into account the MAC of BC and dust for each aerosol bin that are based on calculations performed by SNICAR. The BC and dust mixing ratios for each case are listed with the corresponding BCE values in Table 1.

We first consult measurements taken by Polashenski et al. (2015) from snow pits dug in northwestern Greenland during early summer 2013 and August 2014 to constrain mixing ratios. Although Polashenski et al. (2015) directly measured BC mixing ratios within each snow pit, they were only able to measure mixing ratios of individual ions and element components of dust. Based on previous research and their findings, Polashenski et al. (2015) determined that the ratio of $Ca^{2+}$ to dust concentration ranges from 0.21 to 0.29. Therefore, we multiply their $Ca^{2+}$ mixing ratio measurements by a factor of 4 to infer the dust mixing ratios we impose on the GrIS. Per Polashenski et al. (2015), the lowest BC and dust mixing ratios we use for the IN-SNOW scenario (i.e., BCE = 2.7 ng/g) are representative of average snow pit LAA mixing ratio measurements. The elevated snow pit BCE value based on BC and dust measurements reported by Polashenski

et al. (2015) is 15.7 ng/g, which we use as our second IN-SNOW case. Based on maximum values of additional measurements taken on the GrIS in the early 2000s, we set our third IN-SNOW case BCE as 61.8 ng/g (Bory et al., 2003; McConnell et al., 2007). To achieve a stronger signal and again explore the linearity of climate response to very large mixing ratios of LAA in Greenland snow, we increase the BC and dust mixing ratios from the BCE = 61.8 ng/g run by 50% (BCE = 92.8 ng/g) and 100% (BCE = 123.7 ng/g) for the final IN-SNOW simulations.

Finally, we combine the AOD values from AOD-ONLY scenario with BC and dust mixing ratios from the IN-SNOW cases in the BOTH experiment. Because the AOD-ONLY and IN-SNOW experiments each contain five cases, we match up the associated burdens in each experiment from lowest to highest. The purpose for conducting this suite of runs is to explore the net effects and potential nonlinear responses of atmospheric and in-snow LAA acting in combination, which may differ from the sums of individual impacts identified from AOD-ONLY and IN-SNOW cases. Like in the AOD-ONLY scenario, we maintain SSA = 0.93 for suspended aerosols in all BOTH model runs.

We calculate changes in Greenland's climate attributable to aerosol presence by comparing all of the aforementioned runs to a control simulation. We define this control simulation, termed CONTROL, to have AOD = 0 and an in-snow BCE of 0 ng/g within the Greenland region. The model boundary conditions and specified aerosol concentrations outside of Greenland for CONTROL are the same as the variable runs. For each simulation, we find differences in temperature, snowmelt, and energy fluxes by calculating $\Delta\text{Var} = \text{Var}_{\text{CASE}} - \text{Var}_{\text{CONTROL}}$, where Var is the variable of interest and CASE is one of the non-CONTROL simulations. Furthermore, we test for statistically significant differences between each case and CONTROL by using two-sample $t$ test calculations. This test is done for each grid cell over the Greenland region, as well as on spatially averaged data. All of our statistical calculations involve $n = 10$ summer seasons that are analyzed. For this analysis, we require a confidence interval of 95% for a run to be significantly different from CONTROL ($p \leq 0.05$). To maintain consistency when determining area-weighted spatial averages of the climate state for each case, we filter out sea-based grid cells by using the CESM landfrac field, which provides the fraction of land present in each grid cell. We use a threshold landfrac $\geq 0.83$ to define the land mass of Greenland in order to exclude data from nearby Iceland. In the case of the grid-by-grid statistical analysis, though, we do not take land fraction into account.

## 3. Results and Discussion

In this section, we examine how temperature, snowmelt, and surface energy fluxes change with increasing atmospheric and deposited aerosol loads. First, we compare how air temperature changes vertically with respect to CONTROL for different AOD, SSA, and in-snow LAA mixing ratios. Next, we discuss snowmelt rate changes for the different LAA experiments using two-dimensional difference maps and spatially averaged statistics. We then show how changes in the surface energy balance relative to CONTROL explain simulated differences in snowmelt. Finally, to explain the GrIS-averaged sign of change in surface energy flux, we examine each component of the surface energy balance.

### 3.1. Vertical Temperature Profile Deviations

To gain a better understanding of the different physical mechanisms that lead to changes in melt for all aerosol experiments, we first examine changes in vertical profile air temperature in the lower troposphere. For this portion of the analysis, we average three-dimensional temperature data horizontally over Greenland. The vertical temperature difference ($\Delta T$) plots for all atmospheric and deposited aerosol cases are shown in Figure 1, where the vertical coordinate represents the mean height above the GrIS surface of each hybrid sigma-pressure layer within CAM.

From these plots, we see that increasing atmospheric LAA presence causes localized warming within the aerosol layer as a result of the direct absorption of sunlight. We observe this warming in the AOD-ONLY and VSSA experiments. When we maintain constant SSA in the AOD-ONLY experiment, we find that $\Delta T$ increases monotonically with higher atmospheric aerosol content through the lowest 1.5 km of the troposphere. We determine that decreasing SSA (i.e., increasing aerosol absorptivity) for the VSSA runs also leads to a monotonic increase in $\Delta T$ in the same altitude range. However, temperature change at the surface ($\Delta T_s$) is lower than $\Delta T$ within the aerosol layer because of surface dimming for all AOD-ONLY and VSSA cases. Above
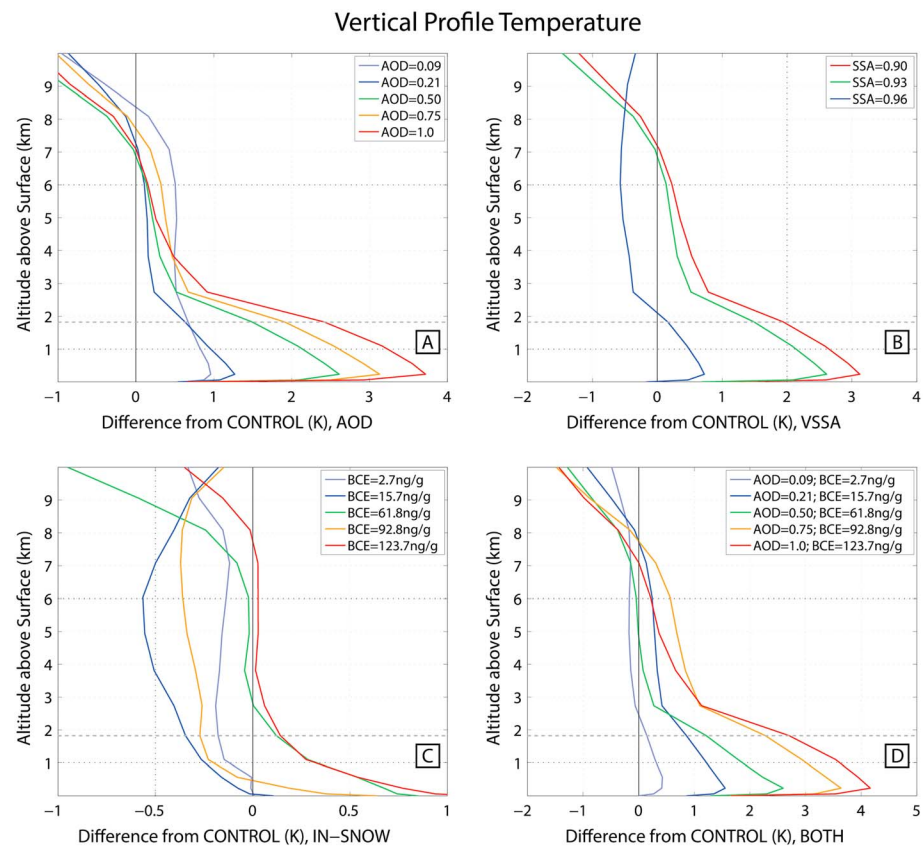
**Figure 1.** Spatially averaged vertical profile difference plots for tropospheric air temperature, relative to CONTROL, for (a) AOD-ONLY, (b) VSSA, (c) IN-SNOW, and (d) BOTH simulations. The horizontal dashed line at ~2 km represents the upper-most LAA altitude for the atmospheric aerosol runs.

the aerosol layer, $\Delta T$ is lower and remains positive through 7 km for all AOD-ONLY cases and the VSSA cases with SSA $\leq 0.93$. The SSA = 0.96 case depicts nonsignificant negative $\Delta T$ just above 2 km because there is less sunlight absorption inside the aerosol layer so less heat energy is transferred to higher altitudes.

In contrast to the AOD-ONLY and VSSA experiments, $\Delta T$ is positive at the surface and decreases with height for all but the smallest of the IN-SNOW runs. With the exception of the BCE = 92.8 ng/g case, we determine that $\Delta T_s$ increases monotonically as we increase BC and dust mixing ratios. Insolation is more readily absorbed at the surface as albedo decreases because of the "in-snow" direct aerosol effect, resulting in surface and lower atmospheric warming. Although we do not observe any surface temperature change for BCE = 2.7 ng/g (i.e., $\Delta T_s \approx 0$), we suspect that this is simply because there is not enough BC and dust in the snow to trigger substantial "in-snow" direct aerosol effect. Despite $\Delta T_s$ being lower for the BCE = 92.8 ng/g case than BCE = 61.8 ng/g, the difference is not statistically significant, so we attribute this nonmonotonic behavior to model noise. For all IN-SNOW runs, we find that only the unreasonably large BCE = 123.7 ng/g case results in significant $\Delta T_s$. Without the effects of atmospheric aerosols in IN-SNOW, $\Delta T$ steadily decreases with altitude because anomalous heating originates at the Earth's surface. We note here that we find negative, decreasing $\Delta T$ with height through most of the atmosphere for BCE = 15.7 ng/g. We attribute this to model noise and variability since no $\Delta T$ are statistically significant.

Like in the AOD-ONLY and VSSA experiments, $\Delta T$ in the BOTH experiment increases monotonically with LAA amount in the aerosol layer and on the surface. All but the AOD = 0.09; BCE = 2.7 ng/g BOTH runs maintain low positive $\Delta T$ from the top of the aerosol layer through 7 km, as we see in AOD-ONLY and VSSA. We calculate larger $\Delta T$ for the BOTH AOD = 1.0; BCE = 123.7 ng/g case than the AOD = 1.0 AOD-ONLY case because of the combined warming effects of atmospheric and deposited LAA.
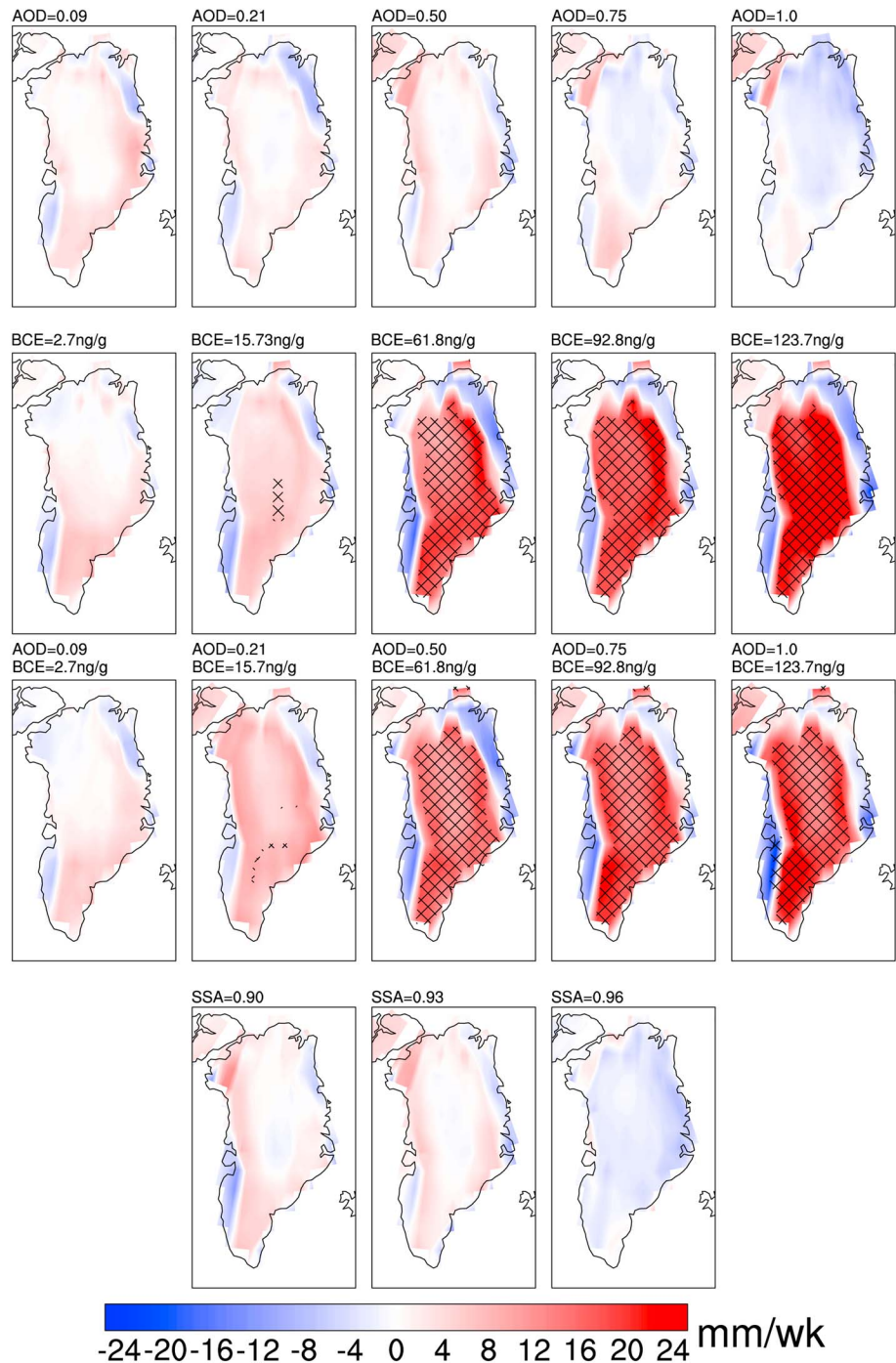
**Figure 2.** ΔQMELT for the (first row) AOD-ONLY, (second row) IN-SNOW, (third row) BOTH, and (fourth row) VSSA experiments.

## 3.2. GrIS Snowmelt (QMELT) Deviations

The $\Delta T$ trends we discuss in the previous section illustrate how suspended and deposited aerosols affect air temperature at the surface and in the lower atmosphere. These $\Delta T$ patterns, along with surface energy flux changes described later, influence snowmelt difference ($\Delta$QMELT) patterns across the GrIS. To explore the

**Figure 3.** Spatially averaged snowmelt (QMELT) and net surface energy ($F_{TOT}$ changes relative to CONTROL for the (a) AOD-ONLY, (b) VSSA, (c) IN-SNOW, and (d) BOTH experiments.

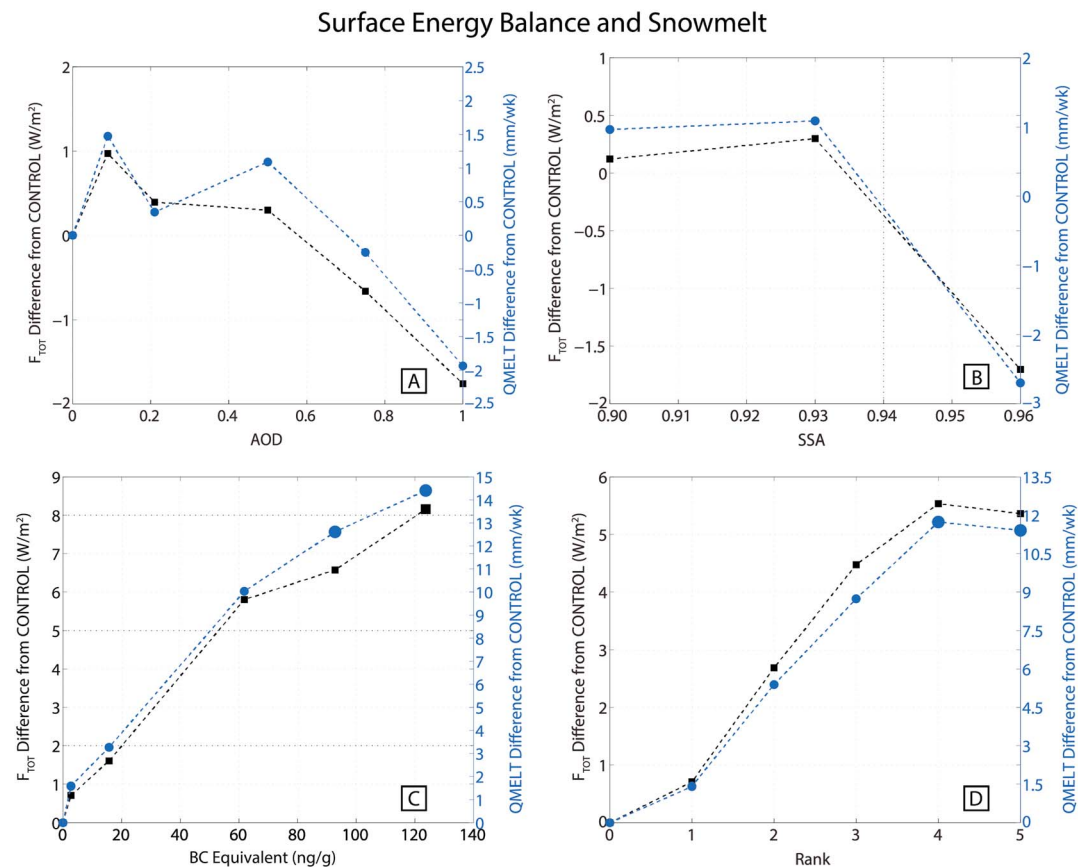ΔQMELT patterns that result when we impose different aerosol loads, we analyze the statistical results and plots of two-dimensional and spatially averaged ΔQMELT (Figures 2 and 3, respectively). We note that there is positive melt on the central GrIS for CONTROL with surface air temperature below 265K (8K below freezing). These QMELT results (not shown) are unusual because the central GrIS rarely experiences melt during the summer months (e.g., Nghiem et al., 2012). We hypothesize that the snowmelt at temperatures below freezing over central Greenland in the model could lead to overestimations of QMELT.

The effect of atmospheric aerosols on ΔQMELT varies based on both aerosol prevalence and SSA. In the AOD-ONLY and VSSA cases, we find that none of the melt patterns are statistically different from CONTROL (Figures 2 and 3). However, despite the small snowmelt changes, certain patterns do emerge with changing AOD and SSA. First, we observe slightly positive ΔQMELT around the periphery of the GrIS for lower AOD values (AOD ≤ 0.50). The enhanced marginal melt rates of the AOD-ONLY runs are caused by a combination of the warming lower troposphere and the absence of substantial surface dimming. We also observe this trend for the SSA = 0.90 and SSA = 0.93 VSSA cases. In contrast to the GrIS margins, however, we observe ΔQMELT ≤ 0 over the central portion of the ice sheet in these AOD-ONLY and VSSA simulations. Even with the direct aerosol effect enhancing air temperature within the aerosol layer, the amount of energy that is transferred to the surface is not large enough to induce positive snowmelt changes. The unrealistically large AOD (i.e., AOD ≥ 0.75) and SSA = 0.96 cases produce mostly negative snowmelt change (i.e., less melting) over the GrIS. For the AOD = 0.75 and AOD = 1.0 runs, the effects of excessive surface dimming and limitations on sensible heat transfer from the warmed atmosphere lead to less total energy reaching the surface (Flanner, 2013). The negative ΔQMELT we observe over the entire GrIS in the SSA = 0.96 case results from increased solar irradiance being scattered by the aerosols away from the surface, combined with minimal atmospheric heating.

## Snow Water Equivalent Differences (H$_2$O-Snow) in JJA
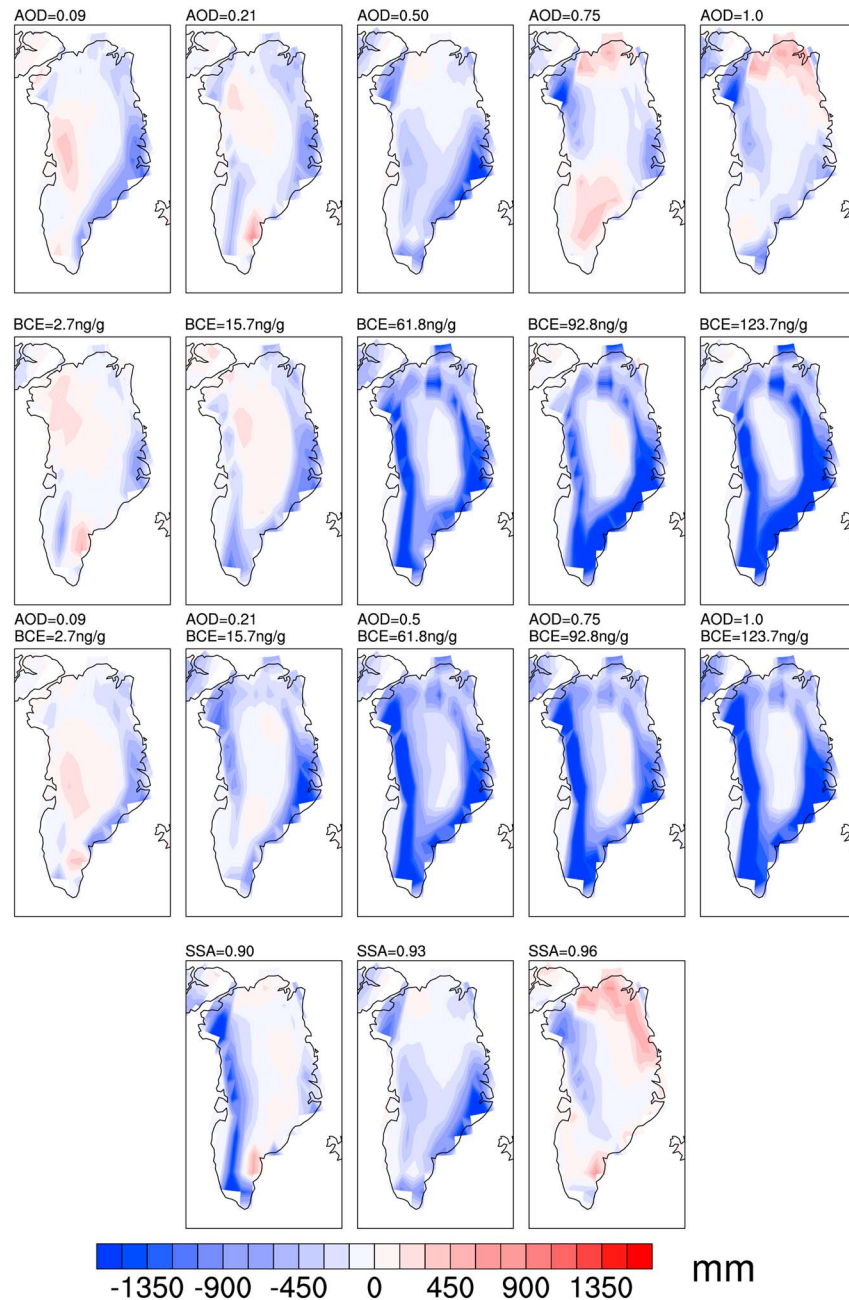


**Figure 4.** Change in GrIS snow water equivalent with respect to CONTROL for the AOD-ONLY, IN-SNOW, BOTH, and VSSA cases.

By increasing in-snow BC and dust mixing ratios, we see that ΔQMELT for the IN-SNOW experiment increases across the GrIS. Furthermore, in all but the lowest IN-SNOW case, significant positive ΔQMELT occurs at some location on the GrIS, with the cases defined by BCE ≥ 61.8 ng/g having significant snowmelt changes almost everywhere. Because deposited LAA lowers the GrIS snow albedo, enhanced melt is expected (e.g., Warren & Wiscombe, 1980). However, based on historical in-snow BC and dust measurements, we emphasize that the high LAA presence associated with cases depicting significant melt on any large scale are very rare. The largest BC mixing ratio measured in a central Greenland ice core dating back to 1788 was 58.8 ng/g and only

occurred once during this time span (McConnell et al., 2007). In our simulations, this corresponds to the BCE = 61.8 ng/g case. We emphasize that the BCE = 92.8 ng/g and BCE = 123.7 ng/g mixing ratios have never been observed in Greenland snow or ice (i.e., Doherty et al., 2010; McConnell et al., 2007; Polashenski et al., 2015). Warming snow and increasing snowmelt also trigger an acceleration of snow aging, where snow grain sizes increase as a result of vapor redistribution, melting and refreezing of water. Enlarged snow grains enable greater albedo perturbation from LAA in snow (Flanner et al., 2007). For all of the IN-SNOW simulations, we find that the northeastern and southwestern margins of the GrIS experience negative ΔQMELT. We determine that this is caused by an average decrease of snow depth (as measured by liquid water depth equivalent; see Figure 4) in the equilibrium state of the simulations. With less snow available for melting, the rate at which melt occurs after reaching equilibrium decreases.

The ΔQMELT spatial patterns and statistical results we find for the BOTH cases are very similar to those of the IN-SNOW experiment. However, despite the strong feedback associated with deposited aerosols, the effects of atmospheric aerosols do reduce the rate at which ΔQMELT increases for the BOTH runs. When we compare ΔQMELT between the IN-SNOW and BOTH simulation suites, $\Delta QMELT_{BOTH} < \Delta QMELT_{IN\_SNOW}$ (compare the lower panels of Figure 3). In the BOTH scenario, some of the surface heating from deposited LAA is counteracted by the dimming effects of atmospheric aerosols. We can see that the magnitude of ΔQMELT across most of the GrIS is slightly lower for the BOTH experiment than the IN-SNOW experiment (Figure 2).

Based on the ΔQMELT trends we see with increasing atmospheric aerosol burden and in-snow aerosol mixing ratios, we can conclude from these modeling experiments that snowmelt of the GrIS is more sensitive to the presence of deposited aerosols than atmospheric aerosols when both are varied similarly in relation to their mean and extreme observed values. We can see from the surface energy balance values shown in Figure 3 that deposited aerosols are more effective at enhancing melt because surface energy flux increases ubiquitously as in-snow LAA mixing ratios are increased. The sign of impact that atmospheric aerosols have on the surface energy balance is less clear because of the competing effects of surface dimming, tropospheric warming, and potential indirect cloud feedbacks.

### 3.3. Surface Energy Budget Changes

Although snowmelt rates respond to changing surface air temperature (compare Figures 1 and 3), the extent to which snow surfaces with temperatures close to melting can warm is limited. However, because large surface energy fluxes can lead to large changes in snowmelt with little change in surface temperature, we expect a more direct relationship between ΔQMELT and net surface energy flux changes ($\Delta F_{TOT}$). To determine $\Delta F_{TOT}$ for each model simulation, we sum the following vector energy quantities at the surface: net solar flux ($\Delta FSNS = \Delta(S^{\downarrow} + S^{\uparrow})$, where $S^{\downarrow}$ and $S^{\uparrow}$ are incoming and outgoing solar energy, respectively), net longwave energy flux ($\Delta FLNS = \Delta(L^{\downarrow} + L^{\uparrow})$ for longwave energy flux, $L$), net sensible heat flux ($\Delta SHFLX$), and net latent heat flux ($\Delta LHFLX$). For each of the energy flux components, we assume that positive energy fluxes are directed at the surface and negative energy fluxes flow upward from the surface (e.g., $S^{\uparrow}$ and $L^{\uparrow}$ are negative in each calculation). We compute the grid-by-grid $\Delta F_{TOT}$ as follows:

$$\Delta F_{TOT} = \Delta FSNS + \Delta FLNS + \Delta SHFLX + \Delta LHFLX. \qquad (2)$$

Although we observe positive SHFLX at the GrIS margins for all cases, different sensible heat flux patterns emerge over the central GrIS. Simulations with little or no atmospheric LAA exhibit negative (i.e., net upward) sensible heat flux over the central GrIS because the overlying air is cooler than the surface because of adiabatic cooling. The cases with high AOD and low SSA maintain positive sensible heat flux over the central GrIS because of the large source of diabatic heating introduced by the suspended LAA. Our model output depicts negative latent heat flow in all simulations that is virtually uniform across the entire GrIS. Because the air above the GrIS is not saturated, ice and water at the surface tends to sublimate or evaporate and lead to negative latent heat flux (Ettema et al., 2010).

As we can see from the Greenland maps, spatially averaged plots, and the statistical results (Figures 5 and 2 and Table 2, respectively), $\Delta F_{TOT}$ and ΔQMELT are very similar for each experiment. For the AOD-ONLY simulations, ΔQMELT and $\Delta F_{TOT}$ initially increase with lower atmospheric aerosol burdens before becoming negative due to strong surface dimming. In the VSSA experiment, average snowmelt and net surface energy decrease with highly scattering atmospheric aerosols but remain slightly positive when SSA ≤ 0.93. In
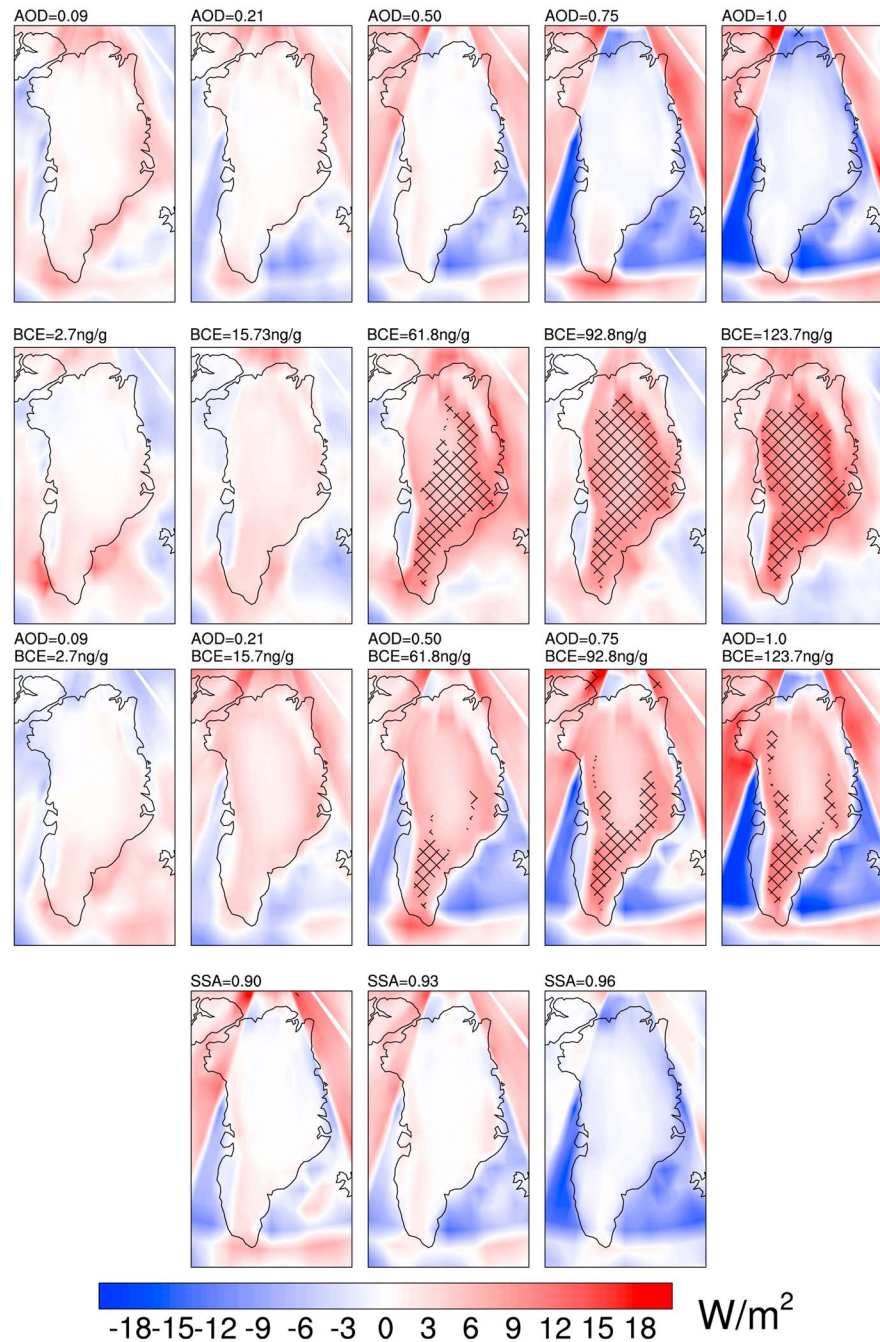
**Figure 5.** $\Delta F_{TOT}$ for the AOD-ONLY, IN-SNOW, BOTH, and VSSA experiments.

contrast to the purely atmospheric aerosol cases, increasing in-snow BC and dust mixing ratios leads to increasing $\Delta QMELT$ and $\Delta F_{TOT}$ as a result of decreasing surface albedo. Based on these results, we can state with a good degree of certainty that changes in surface energy dictate melt pattern changes. However, the changes in each energy component with additional aerosol cannot be determined from this information alone. We can use the relative magnitudes of solar and turbulent energy fluxes in $\Delta F_{TOT}$ to determine how each of these fluxes are influenced by changes in LAA abundance, location, and optical properties (Figure 6).

**Table 2**
*Net Surface Energy Component Differences*[a]

| Experiment | | ΔFSNS | | ΔFLNS | | ΔSHFLX | ΔLHFLX |
|---|---|---|---|---|---|---|---|
| Aerosol Scenario | Case | $\Delta S^{\uparrow}$ | $\Delta S^{\downarrow}$ | $\Delta L^{\uparrow}$ | $\Delta L^{\downarrow}$ | -- | -- |
| AOD-ONLY (AOD=) (for SSA = 0.93) | 0.09 | | 0.93 | | −1.53 | 1.20 | 0.36 |
| | | 6.98 | −6.04 | −2.64 | 1.11 | -- | -- |
| | 0.21 | | 0.24 | | −2.82 | 2.02 | 0.95 |
| | | 12.95 | −12.71 | −2.36 | −0.46 | -- | -- |
| | 0.50 | | −0.25 | | −6.59 | 4.61 | 2.53 |
| | | 24.50 | −24.75 | −3.05 | −3.54 | -- | -- |
| | 0.75 | | −4.13 | | −5.52 | 5.53 | 3.67 |
| | | 34.11 | −38.24 | −2.96 | −2.56 | -- | -- |
| | 1.0 | | −5.49 | | −6.55 | 6.43 | 4.21 |
| | | 42.42 | −48.27 | −2.87 | −3.69 | -- | -- |
| VSSA (SSA=) (for AOD = 0.50) | 0.90 | | −2.19 | | −5.24 | 4.60 | 2.95 |
| | | 32.09 | −34.28 | −4.50 | −0.74 | -- | -- |
| | 0.96 | | −4.90 | | −1.22 | 2.47 | 1.95 |
| | | 19.62 | −24.52 | 0.65 | −1.87 | -- | -- |
| IN-SNOW (BCE (ng/g)=) | 2.7 | | 3.21 | | −1.86 | −0.43 | −0.21 |
| | | 0.31 | 2.91 | −0.08 | −1.77 | -- | -- |
| | 15.7 | | 3.81 | | −0.23 | −1.39 | −0.59 |
| | | 7.46 | −3.65 | −0.49 | 0.27 | -- | -- |
| | 61.8 | | 11.65 | | −2.38 | −1.61 | −1.86 |
| | | 18.87 | −7.22 | −3.78 | 1.39 | -- | -- |
| | 92.8 | | 11.52 | | −0.62 | −2.39 | −1.95 |
| | | 23.69 | −12.16 | −2.81 | 2.19 | -- | -- |
| | 123.7 | | 14.50 | | −1.37 | −2.60 | −2.37 |
| | | 28.37 | −13.87 | −5.16 | 3.79 | -- | -- |
| BOTH (AOD, BCE (ng/g)=) | 0.09; 2.7 | | 1.99 | | −2.60 | 0.89 | 0.43 |
| | | 5.92 | −3.93 | −0.06 | −2.53 | -- | -- |
| | 0.21; 15.7 | | 3.13 | | −2.68 | 1.42 | 0.82 |
| | | 19.11 | −15.98 | −3.78 | 1.09 | -- | -- |
| | 0.50; 61.8 | | 7.29 | | −6.13 | 2.15 | 1.16 |
| | | 39.36 | −32.07 | −5.62 | −0.51 | -- | -- |
| | 0.75; 92.8 | | 5.36 | | −5.82 | 3.62 | 2.38 |
| | | 51.97 | −46.61 | −7.18 | 1.36 | -- | -- |
| | 1.0; 123.7 | | 6.20 | | −8.07 | 4.39 | 2.84 |
| | | 60.45 | −54.24 | −7.23 | −0.84 | -- | -- |

[a]Differences (in units of W/m$^2$) are with respect to CONTROL. Positive ΔFSNS, ΔFLNS, ΔSHFLX, and ΔLHFLX depict energy flow into the surface. The gray boxes highlight statistical significance. $\Delta S^{\uparrow} < 0$ and $\Delta L^{\uparrow} < 0$ indicate increased upwelling in the variable case, while $\Delta S^{\downarrow} < 0$ and $\Delta L^{\downarrow} < 0$ indicate less downwelling energy.

Increasing the mass of LAA in the atmosphere generally leads to negative ΔFSNS through the process of surface dimming (Figure 6a). As expected, spatially averaged ΔFSNS (red line) values are negative when AOD ≥ 0.5 in the AOD-ONLY simulations. Unexpectedly, in spite of the increasing LAA burden in the atmosphere, the AOD = 0.09 and AOD = 0.21 cases (Figure 6) exhibit positive ΔFSNS. This occurs in the model because these aerosols lead to so-called cloud burn-off while simultaneously allowing most of the insolation to transmit through the sparsely concentrated aerosol layer (Ban-Weiss et al., 2011; Ramanathan & Carmichael, 2008). We can verify cloud burn-off by calculating the change in cloud radiative effect (ΔCRE) between each AOD-ONLY case and CONTROL:

$$\Delta CRE = \Delta FSNSC - \Delta FSNS \tag{3}$$

where FSNSC is clear-sky solar flux. Negative ΔCRE indicates higher cloud radiative effect in CONTROL. High-latitude clouds are difficult to model because cloud phase, optical thickness, and altitude result from the
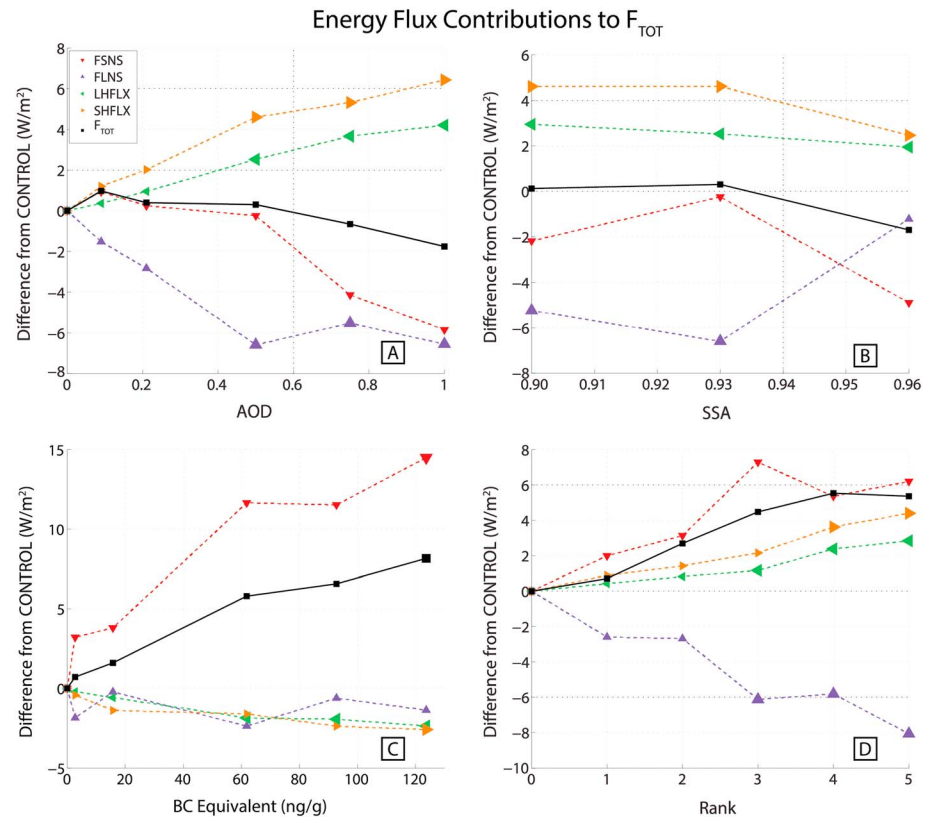
**Figure 6.** Spatially averaged surface energy flux component changes for (a) AOD-ONLY, (b) VSSA, (c) IN-SNOW, and (d) BOTH scenarios. In each plot, FSNS is the net solar energy, FLNS is the net longwave energy, SHFLX is sensible heat flux, and LHFLX is latent heat flux.

combination of large-scale circulation, boundary layer, and microphysical processes, among others (Curry et al., 1996; Kay & Gettelman, 2009). de Boer et al. (2012) and Kay et al. (2012) determined that cloud fraction is underestimated in the Arctic at all altitudes in CAM4. de Boer et al. (2012) also determined that liquid water path was overestimated and ice water path was underestimated by CAM4 in the high latitudes. We hypothesize that these cloud biases could impact our assessment of cloud changes and surface energy balance over Greenland. Based on de Boer et al. (2012) cloud composition findings in CAM4, we can assume that liquid clouds are over-represented in our simulations. Liquid clouds are more reflective than ice clouds, so CONTROL clouds might have a high-albedo bias. We speculate that burn-off of these liquid clouds could lead to overestimated $\Delta S^{\downarrow}$ and net surface energy changes. Bearing these potential cloud biases in mind, we see low-level cloud burn-off for the AOD = 0.09 and AOD = 0.21 runs relative to CONTROL in Figure 7 and in $\Delta$CRE calculations (i.e., $\Delta$CRE$_{AOD = 0.09}$ = − 1.6 W/m$^2$ and $\Delta$CRE$_{AOD = 0.21}$ = − 3.6 W/m$^2$). This is further supported by the FLNS results we discuss later in this section. We also observe lower surface albedo and upwelling solar energy in these cases (not shown), suggesting that decreasing GrIS snow albedo leads to enhanced absorption of sunlight at the surface. We speculate that these changes result from snow aging processes induced by elevated $S^{\downarrow}$, whereby snow grains become larger and result in lower near-infrared surface albedo (e.g., Flanner & Zender, 2006).

Like the AOD-ONLY cases with AOD $\geq$ 0.50, we determine that $\Delta$FSNS is negative for all of the VSSA cases (Figure 6b). Given that AOD = 0.50 for all of the VSSA runs, we know that surface dimming causes the reduction of sunlight at the surface. However, the mechanism diverting energy away from the GrIS depends on aerosol SSA. We find that $\Delta S^{\uparrow}$ (Table 2) is more positive (i.e., there is less upwelling energy in the variable case) and $\Delta S^{\downarrow}$ is more negative (i.e., there is less downwelling energy) for the SSA = 0.90 case due to enhanced LAA absorption. The values of $\Delta S^{\uparrow}$ and $\Delta S^{\downarrow}$ are roughly the same magnitude for SSA = 0.90, so its resulting $\Delta$FSNS is less negative than $\Delta$FSNS for SSA = 0.96.
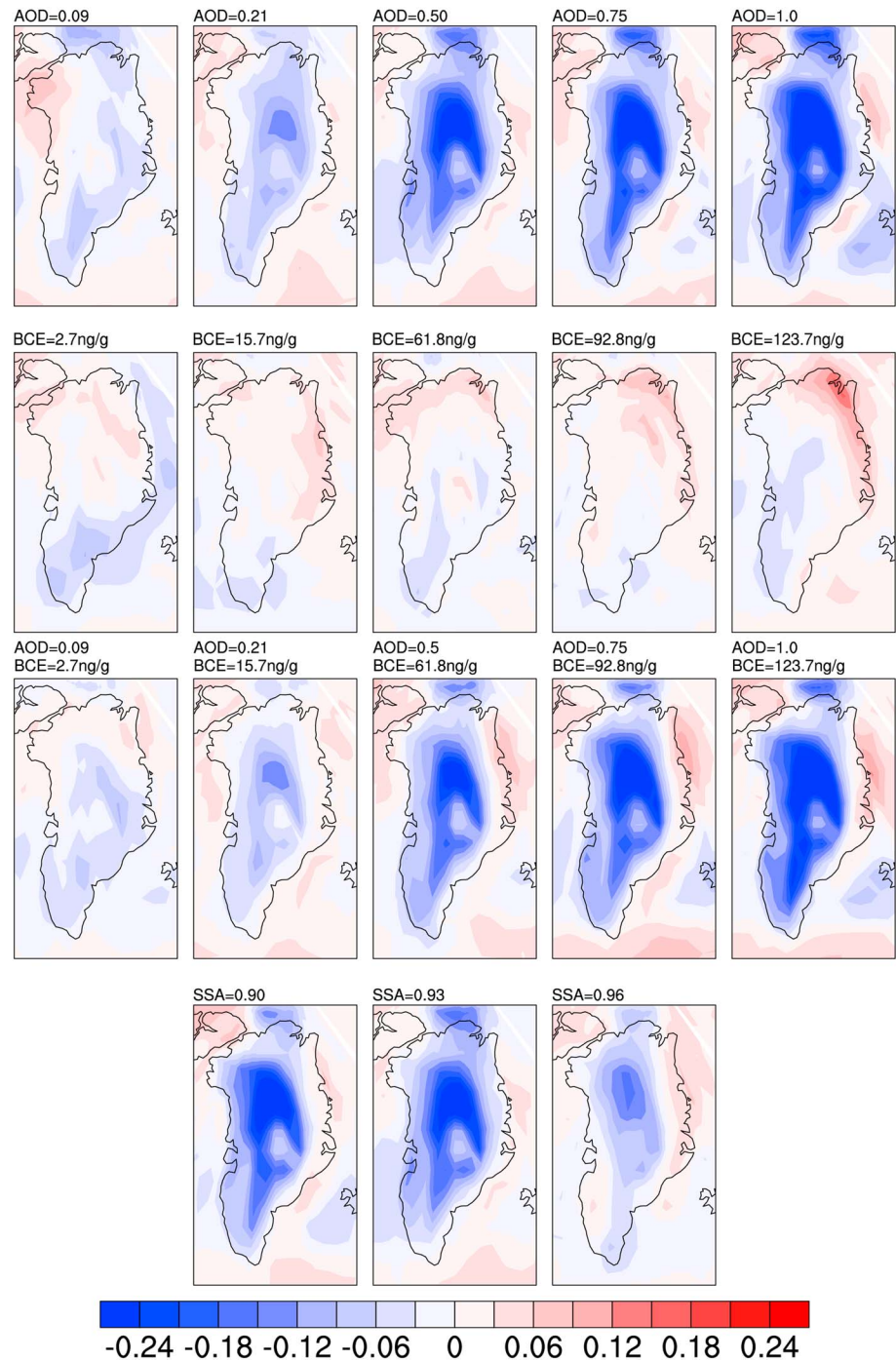
**Figure 7.** Low cloud fraction changes for all cases relative to CONTROL.

In contrast to the atmospheric aerosol cases, the effects of deposited LAA on ΔFSNS are more straightforward (Figure 6c). As we see from the IN-SNOW ΔQMELT and Δ$T$ results, ΔFSNS becomes more positive with enhanced BC and dust mixing ratios due to the "in-snow" direct aerosol effect. Similarly, despite simultaneous atmospheric LAA presence, ΔFSNS also increases with enhanced aerosol burdens in the BOTH experiment. This further demonstrates that the presence of deposited BC and dust is generally more influential on the amount of solar energy absorbed at the surface than the presence of suspended LAA.

However, when we compare ΔFSNS between the IN-SNOW and BOTH experiments, we see that the largest ΔFSNS value in the BOTH runs (Figure 6d) is not statistically significant and is roughly half the magnitude of the largest ΔFSNS for IN-SNOW. This results from the competing effects of surface dimming and surface darkening present in the BOTH experiment. We determine that IN-SNOW ΔFSNS is highest with the largest BC and dust mixing ratios, but because of dimming, the BOTH case with the highest ΔFSNS is AOD = 0.50; BCE = 61.8 ng/g. These results suggest that the net impact of LAA is lower when both atmospheric and deposited aerosols are acting. The effects of deposited (atmospheric) LAA at high latitudes are often modeled independently; we assert that neglecting atmospheric (deposited) LAA in model simulations may lead to nonnegligible biases in net surface energy flux.

For all of the experiments, we determine that average ΔFLNS (purple line) negatively contributes to $\Delta F_{TOT}$. The upwelling longwave term, $L^{\uparrow}$, responds to surface temperature changes via the Stefan-Boltzmann relationship. However, the downwelling longwave energy flux change patterns ($L^{\downarrow}$) depend on aerosol location. In all but the AOD = 0.09 case, we find negative $\Delta L^{\downarrow}$. Although the LAA lead to localized warming in the atmosphere that could cause positive $\Delta L^{\downarrow}$, the low-level (Figure 7) and midlevel cloud burn-off that result from the LAA reduce cloud-based $L^{\downarrow}$. The negative $\Delta L^{\downarrow}$ values that we calculate in the AOD-ONLY and VSSA experiments suggest that the effect of cloud removal slightly outweighs that of tropospheric warming.

When we examine the deposited aerosol cases (i.e., IN-SNOW and BOTH), we find that the magnitude of ΔFLNS largely depends on the presence of atmospheric LAA. As we observe in the IN-SNOW cases, ΔFLNS is negative and remains mostly constant. Similar to the AOD-ONLY and VSSA experiments, BOTH ΔFLNS becomes more negative as the atmospheric aerosol burden increases. The highest BC and dust mixing ratio cases in IN-SNOW and BOTH show the BOTH case having a ΔFLNS magnitude that is at least three times larger than the IN-SNOW equivalent. When we compare cloud burn-off between all experiments, we find the smallest low-level cloud fraction change in the IN-SNOW cases. Therefore, cloud-based $L^{\downarrow}$ in the IN-SNOW runs does not decrease to the extent that we observe in the other cases (Figure 7). Furthermore, unlike the atmospheric aerosol experiments, IN-SNOW ΔFLNS only depends on BC and dust mixing ratios; the GrIS surface does not receive any statistically significant change in $L^{\downarrow}$ from the atmosphere relative to CONTROL.

Unlike the shortwave and longwave energy fluxes, increasing AOD and decreasing SSA lead to positive ΔSHFLX (orange line) and ΔLHFLX (green line; i.e., more downward directed flux or less upward directed flux). Both of these changes occur as a result of the direct aerosol effect. With increasing atmospheric LAA burdens or decreasing SSA, more insolation is absorbed in the aerosol layer. As we have seen with the $\Delta T$ analysis, this leads to increasing $\Delta T$ within the aerosol layer. By the Clausius-Clapeyron relationship, local saturation specific humidity also increases. These air temperature and saturation specific humidity enhancements lead to positive sensible and latent heat flux changes. Research by Wang (2004) also supports this positive change in heat energy flux as a result of LAA presence. Wang (2004) used a suite of global climate models to determine how BC affects radiative energy in the climate system. In response to negative radiative forcing at the surface caused by BC in the atmosphere, Wang (2004) suggested that the positive sensible and latent heat fluxes served as a compensating mechanism to offset the negative energy balance at the surface. This result is apparent in our AOD-ONLY and VSSA model simulations. In the AOD-ONLY and VSSA scenarios, ΔSHFLX and ΔLHFLX are the only positive energy components of $\Delta F_{TOT}$. However, as we can observe from Figures 6a and 6b, the negative ΔFSNS and ΔFLNS are collectively comparable to ΔSHFLX and ΔLHFLX. This is why we do not calculate significant ΔQMELT or $\Delta F_{TOT}$ in any of these cases.

Deposited aerosols in IN-SNOW lead to changes in the magnitude and sign of ΔSHFLX and ΔLHFLX relative to the BOTH runs. To compensate for energy being added to the surface via positive ΔFSNS, the IN-SNOW simulations exhibit negative ΔSHFLX and ΔLHFLX. Air temperature and specific humidity increase at the surface (e.g., Figure 1) relative to CONTROL and create changes in temperature and specific humidity gradients that lead to negative heat flux changes. As we can see from Figure 6, the values of ΔSHFLX and ΔLHFLX for IN-SNOW decrease slightly with increasing deposited LAA mixing ratios and are comparable to the magnitude of ΔFLNS. Overall, the only positive energy contribution to $\Delta F_{TOT}$ for IN-SNOW is ΔFSNS. However, ΔFSNS for each BC and dust mixing ratio case is much larger than the sum of ΔFLNS, ΔSHFLX, and ΔLHFLX, which is why $\Delta F_{TOT}$ and ΔQMELT are positive for all IN-SNOW cases.

In contrast to the IN-SNOW experiment, the BOTH simulations all depict positive $\Delta$SHFLX and $\Delta$LHFLX. This indicates that for surface sensible and latent heat flux changes, atmospheric aerosols are more influential on the direction of energy flow than their in-snow counterparts. We also note that of all of the experiments involving atmospheric aerosols, $\Delta$SHFLX and $\Delta$LHFLX magnitudes are the smallest in the BOTH scenario because of the offsetting impacts of in-snow aerosols. However, despite positive $\Delta$SHFLX and $\Delta$LHFLX for all BOTH cases, we can see from Figure 6 that solar energy changes still contribute more to $\Delta F_{TOT}$. Unlike all of the other simulations, the only surface energy component that leads to energy depletion in $\Delta F_{TOT}$ in BOTH is $\Delta$FLNS. However, the combination of $\Delta$FSNS, $\Delta$SHFLX, and $\Delta$LHFLX all contribute more energy to the surface than longwave energy emission removes, so $\Delta$QMELT and $\Delta F_{TOT}$ both increase.

## 4. Conclusion

In this study, we use CESM to better understand the relative impact of atmospheric and deposited LAA on the climate of Greenland. To achieve this goal, we compare idealized simulations with varying LAA mixing ratios to a local-to-Greenland no-aerosol control run (i.e., CONTROL) by using a series of independent two-sample $t$ tests. By comparing variable aerosol simulations to CONTROL, we are able to determine the effects of LAA on the climate of Greenland, and we are also able to determine how increasing aerosol burdens can impact these results.

We determine that air temperature changes ($\Delta T$) throughout the lower portion of the atmosphere and at the surface are caused by local LAA. In the AOD-ONLY runs, air temperature within the aerosol layer and at the surface increases monotonically with respect to CONTROL. However, $\Delta T_s$ is smaller than $\Delta T$ within the aerosol layer for all AOD-ONLY cases because of surface dimming caused by the suspended LAA. We observe the same $\Delta T$ patterns seen in the AOD-ONLY cases at both the surface and in the lower troposphere for the VSSA runs. We further determine that decreasing SSA leads to a monotonic increase in $\Delta T$ as a result of the increasing absorbing capabilities of the LAA. Deposited aerosols also affect the $\Delta T$ trends we observe, but the patterns differ from those we see with atmospheric aerosols. With the exception of the BCE = 92.8 ng/g case in the IN-SNOW experiment, $\Delta T_s$ increases monotonically because of the "in-snow" direct aerosol effect. We attribute the nonmonotonic $\Delta T_s$ increase for the BCE = 92.8 ng/g run to model noise and variability. We also demonstrate that $\Delta T$ decreases in magnitude with altitude for all IN-SNOW runs. When we simulate the presence of both atmospheric and deposited LAA, the resulting air temperature change trends are similar to those in AOD-ONLY, but the $\Delta T$ values are positively skewed in the lower troposphere and at the surface for higher LAA cases.

Along with the changes in tropospheric air temperature, we determine that snowmelt and surface energy flux changes associated with LAA largely depend on aerosol location. Increasing atmospheric LAA burden leads to surface dimming and enhanced air temperatures just above the surface. These offsetting effects of atmospheric LAA lead to nonstatistically significant changes in melt and net surface energy flux across the entire GrIS for the AOD-ONLY and VSSA experiments. For the AOD-ONLY cases, we show that both snowmelt and net surface energy flux initially increase with enhanced LAA burden before decreasing as a result of surface dimming. We find further evidence of surface dimming by the negative $\Delta$FSNS component of $\Delta F_{TOT}$ when AOD $\geq$ 0.50. In contrast, we calculate positive $\Delta$FSNS in the AOD $\leq$ 0.21 cases because of cloud burn-off. Although the sign of $\Delta$FSNS for the AOD-ONLY experiment depends on the AOD value, we observe that both $\Delta$FSNS and snowmelt changes ($\Delta$QMELT) transform from positive to negative at the same AOD value. This indicates that $\Delta$FSNS is very influential for subsequent snowmelt changes. The change in net longwave energy flux negatively impacts the surface energy balance for all atmospheric aerosol cases. In contrast, $\Delta$SHFLX and $\Delta$LHFLX positively contribute to $\Delta F_{TOT}$ as a result of localized warming in the air above the GrIS. We observe this pattern in all experiments involving the presence of atmospheric aerosols, regardless of whether in-snow impurities are also present. In the VSSA experiment, $\Delta$FSNS is negative for all cases because of absorption or scattering by the moderately high aerosol load imposed in the lower troposphere. As a result of decreased surface albedo from in-snow LAA overwhelming dimming caused by atmospheric LAA, though, the BOTH simulations all maintain positive $\Delta$FSNS.

When we impose BC and dust in GrIS snow, we find that snowmelt and net surface energy increase with increasing LAA mixing ratios because of reduced surface albedo. In the IN-SNOW and BOTH experiments, snowmelt increases with higher aerosol burdens. Unlike the BOTH scenario, the IN-SNOW positive energy

balance of the GrIS is due to the dominating positive ΔFSNS relative to negative ΔFLNS, ΔSHFLX, and ΔLHFLX. The relative magnitudes of ΔQMELT for the IN-SNOW runs are comparable to the corresponding FSNS deviations, while changes in snowmelt for the BOTH experiment depend on ΔFSNS, and to a lesser extent, ΔSHFLX and ΔLHFLX. Overall, we find that in-snow aerosols affect snowmelt more than their atmospheric counterparts. However, the snowmelt and net surface energy changes we calculate for these experiments show that LAA in the atmosphere reduce the impact of aerosols on the ground by a factor of 2. This finding highlights the offsetting effects of atmospheric aerosols and emphasizes the importance of including atmospheric LAA when simulating the climate effects of deposited LAA, especially on ice- and snow-covered terrain.

Although this research demonstrates the relative effects of atmospheric and deposited LAA on air temperature, snowmelt, and surface energy fluxes for the GrIS, there are several aspects of Greenland's climate and the effects of biomass burning that we do not address. Most importantly, we investigate the effects of LAA in a highly idealized modeling environment. We maintain constant and spatially uniform aerosol burdens in the snow and lower atmosphere for the duration of each simulation rather than explicitly representing aerosol advection from remote locations into the Greenland region (e.g., Thomas et al., 2017). Atmospheric circulation mechanisms lead to spatially heterogeneous aerosol distributions on the surface and in the atmosphere. For example, atmospheric LAA from biomass burning generally decrease from west to east over the GrIS because of plume dilution and LAA depositional processes. Although BC and OC can serve as CCN after transport and aging processes (i.e., Bond et al., 2013), the bulk aerosol setup we use neglects this process. BC and OC CCN affect cloud lifespan, cloud albedo, and incident radiation at the surface. Wang et al. (2018) confirm that aerosol microphysical effects make up a large portion of the total aerosol forcing in the Arctic. Inclusion of these effects in our experimental setup would have impacted our findings. Along with simulating spatially homogeneous aerosol burdens, the larger atmospheric and in-snow aerosol mixing ratios we impose (i.e., rank 4 and rank 5 on Table 1) are extreme burdens that have not been observed over Greenland (McConnell et al., 2007; Polashenski et al., 2015). LAA mixing ratios similar to the BCE = 61.8 ng/g case have only been measured in GrIS snow once during the last 215 years, and monthly concentrations of BC in GrIS snow that exceed 5 ng/g have occurred only two or three times in each decade since 1950 (McConnell et al., 2007). Because biomass burning and its transport are spatially and temporally episodic, simulating the constant presence of biomass burning aerosols over and on the surface of Greenland leads to more radiative forcing than would be realistic for the region (Clark et al., 2015). However, regardless of emission source, multiple studies have found that BC and other aerosols are most prevalent over the GrIS during the summer months (Jiao et al., 2014; Sand et al., 2013). Biomass burning and anthropogenic aerosols transported to the GrIS from other areas of the northern hemisphere are suspended at various levels in the atmosphere (e.g., Jiao & Flanner, 2016), which we also do not take into account for our atmospheric aerosol experiments.

Although the purpose of this study is to explore Greenland's climate response to idealized, clearly defined distributions of LAA, it would be noteworthy to take these factors into account to depict a more realistic representation of the response of Greenland's climate. Furthermore, in the case of our experimental setup, it would also be useful to examine the effects of LAA SSA by expanding SSA deviations to AOD values apart from AOD = 0.50. Overall, the results from these idealized and well-defined experiments indicate that BC and dust can affect snowmelt and the climate of Greenland when suspended in the atmosphere or, especially, deposited on the surface.

## References

Ban-Weiss, G. A., Cao, L., Bala, G., & Caldeira, K. (2011). Dependence of climate forcing and response on the altitude of black carbon aerosols. *Climate Dynamics*, *38*(5-6), 897–911. https://doi.org/10.1007/s00382-011-1052-y

Bond, T. C., Charlson, R. J., & Heintzenburg, J. (1998). Quantifying the emission of light-absorbing particles: Measurements tailored to climate studies. *Geophysical Research Letters*, *25*(3), 337–340. https://doi.org/10.1029/98GL00039

Bond, T. C., Doherty, S. J., Fahey, D. W., Forster, P. M., Berntsen, T., DeAngelo, B. J., et al. (2013). Bounding the role of black carbon in the climate system: A scientific assessment. *Journal of Geophysical Research: Atmospheres*, *118*, 5380–5552. https://doi.org/10.1002/jgrd.50171

Bory, A. J.-M., Biscaye, P. E., Piotrowski, A. M., & Steffensen, J. P. (2003). Regional variability of ice core dust composition and provenance in Greenland. *Geochemistry, Geophysics, Geosystems*, *4*(12), 1107. https://doi.org/10.1029/2003GC000627

Chung, S. H., & Seinfeld, J. H. (2002). Global distribution and climate forcing of carbonaceous aerosols. *Journal of Geophysical Research*, *107*(D19), 4407. https://doi.org/10.1029/2001JD001397

Clark, S. K., Ward, D. S., & Mahowald, N. M. (2015). The sensitivity of global climate to the episodicity of fire aerosol emissions. *Journal of Geophysical Research: Atmospheres*, *120*, 11,589–11,607. https://doi.org/10.1002/2015JD024068

Curry, J. A., Rossow, W. B., Randall, D., & Schramm, J. L. (1996, August). Overview of Arctic cloud and radiation characteristics. *Journal of Climate*, *9*(8), 1731–1764. https://doi.org/10.1175/1520-0442(1996)009%3C1731:OOACAR%3E2.0.CO;2

de Boer, G., Chapman, W., Kay, J. E., Medeiros, B., Shupe, M. D., Vavrus, S., & Walsh, J. (2012). A characterization of the present-day Arctic atmosphere in CCSM4. *Journal of Climate*, *25*(8), 2676–2695. https://doi.org/10.1175/JCLI-D-11-00228.1

Doherty, S. J., Warren, S. G., Grenfell, T. C., Clarke, A. D., & Brandt, R. E. (2010). Light-absorbing impurities in Arctic snow. *Atmospheric Chemistry and Physics*, *10*(23), 11,647–11,680. https://doi.org/10.5194/acp-10-11647-2010

Ettema, J., van den Broeke, M. R., van Meijgaard, E., & van de Berg, W. J. (2010). Climate of the Greenland ice sheet using a high-resolution climate model—Part 2: Near-surface climate and energy balance. *The Cryosphere*, *4*(4), 529–544. https://doi.org/10.5194/tc-4-529-2010

Flanner, M. G. (2013). Arctic climate sensitivity to local black carbon. *Journal of Geophysical Research: Atmospheres*, *118*, 1840–1851. https://doi.org/10.1002/jgrd.50176

Flanner, M. G., & Zender, C. S. (2005). Snowpack radiative heating: Influence on Tibetan Plateau climate. *Geophysical Research Letters*, *32*, L06501. https://doi.org/10.1029/2004GL022076

Flanner, M. G., & Zender, C. S. (2006). Linking snowpack microphysics and albedo evolution. *Journal of Geophysical Research*, *111*, D12208. https://doi.org/10.1029/2005JD006834

Flanner, M. G., Zender, C. S., Randerson, J. T., & Rasch, P. J. (2007). Present-day climate forcing and response from black carbon in snow. *Journal of Geophysical Research*, *112*, D11202. https://doi.org/10.1029/2006JD008003

Flannigan, M., Cantin, A. S., de Groot, W. J., Wotton, M., Newbery, A., & Gowman, L. M. (2013). Global wildland fire season severity in the 21st century. *Forest Ecology and Management*, *294*, 54–61. https://doi.org/10.1016/j.foreco.2012.10.022

Flannigan, M. D., Krawchuk, M. A., de Groot, W. J., Wotton, B. M., & Gowman, L. M. (2009). Implications of changing climate for global wildland fire. *International Journal of Wildland Fire*, *18*(5), 483–507. https://doi.org/10.1071/WF08187

Gregory, J. M., Huybrechts, P., & Raper, S. C. B. (2004). Climatology: Threatened loss of the Greenland ice-sheet. *Nature*, *428*(6983), 616. https://doi.org/10.1038/428616a

Hanna, E., Huybrechts, P., Steffen, K., Cappelen, J., Huff, R., Shuman, C., et al. (2008). Increased runoff from melt from the Greenland Ice Sheet: A response to global warming. *Journal of Climate*, *21*(2), 331–341. https://doi.org/10.1175/2007JCLI1964.1

Hansen, J., & Nazarenko, L. (2004). Soot climate forcing via snow and ice albedos. *Proceedings of the National Academy of Sciences of the United States of America*, *101*(2), 423–428. https://doi.org/10.1073/pnas.2237157100

Haywood, J. M., & Ramaswamy, V. (1998). Global sensitivity studies of the direct radiative forcing due to anthropogenic sulfate and black carbon aerosols. *Journal of Geophysical Research*, *103*(D6), 6043–6058. https://doi.org/10.1029/97JD03426

Jacobson, M. Z. (2001). Global direct radiative forcing due to multicomponent anthropogenic and natural aerosols. *Journal of Geophysical Research*, *106*(D2), 1551–1568. https://doi.org/10.1029/2000JD900514

Jacobson, M. Z. (2004). Climate response of fossil fuel and biofuel soot, accounting for soot's feedback to snow and sea ice albedo and emissivity. *Journal of Geophysical Research*, *109*, D21201. https://doi.org/10.1029/2004JD004945

Jiao, C., & Flanner, M. G. (2016). Changing black carbon transport to the Arctic from present day to the end of the 21st century. *Journal of Geophysical Research: Atmospheres*, *121*, 4734–4750. https://doi.org/10.1002/2015JD023964

Jiao, C., Flanner, M. G., Balkanski, Y., Bauer, S. E., Bellouin, N., Berntsen, T. K., et al. (2014). An AeroCom assessment of black carbon in Arctic snow and sea ice. *Atmospheric Chemistry and Physics*, *14*(5), 2399–2417. https://doi.org/10.5194/acp-14-2399-2014

Jolly, W. M., Cochrane, M. A., Freeborn, P. H., Holden, Z. A., Brown, T. J., Williamson, G. J., & Bowman, D. M. J. S. (2015). Climate-induced variations in global wildfire danger from 1979 to 2013. *Nature Communications*, *6*(1), 7537. https://doi.org/10.1038/ncomms8537

Kay, J. E., & Gettelman, A. (2009). Cloud influence on and response to seasonal Arctic sea ice loss. *Journal of Geophysical Research*, *114*, D18204. https://doi.org/10.1029/2009JD011773

Kay, J. E., Hillman, B. R., Klein, S. A., Zhang, Y., Medeiros, B., Pincus, R., et al. (2012). Exposing global cloud biases in the Community Atmosphere Model (CAM) using satellite observations and their corresponding instrument simulators. *Journal of Climate*, *25*(15), 5190–5207. https://doi.org/10.1175/JCLI-D-11-00469.1

Keegan, K. M., Albert, M. R., McConnell, J. R., & Baker, I. (2014). Climate change and forest fires synergistically drive widespread melt events of the Greenland Ice Sheet. *Proceedings of the National Academy of Sciences of the United States of America*, *111*(22), 7964–7967. https://doi.org/10.1073/pnas.1405397111

Kelly, R., Chipman, M. L., Higuera, P. E., Stefanova, I., Brubaker, L. B., & Hu, F. S. (2013, August). Recent burning of boreal forests exceeds fire regime limits of the past 10,000 years. *Proceedings of the National Academy of Sciences of the United States of America*, *110*(32), 13,055–13,060. https://doi.org/10.1037/pnas.1305069110

Koch, D., Schulz, M., Kinne, S., McNaughton, C., Spackman, J. R., Balkanski, Y., et al. (2009). Evaluation of black carbon estimations in global aerosol models. *Atmospheric Chemistry and Physics*, *9*(22), 9001–9026. https://doi.org/10.5194/acp-9-9001-2009

Lamarque, J.-F., Bond, T. C., Eyring, V., Granier, C., Heil, A., Klmont, Z., et al. (2010). Historical (1850-2000) gridded anthropogenic and biomass burning emissions of reactive gases and aerosols: Methodology and application. *Atmospheric Chemistry and Physics*, *10*(15), 7017–7039. https://doi.org/10.5194/acp-10-7017-2010

Liu, X., Easter, R. C., Ghan, S. J., Zaveri, R., Rasch, P., Shi, X., et al. (2012). Toward a minimal representation of aerosols in climate models: Description and evaluation in the Community Atmosphere Model CAM5. *Geoscientific Model Development*, *5*(3), 709–739. https://doi.org/10.5194/gmd-5-709-2012

Marlon, J. R., Bartlein, P. J., Daniau, A.-L., Harrison, S. P., Maezumi, S. Y., Power, M. J., et al. (2013). Global biomass burning: A synthesis and review of Holocene paleofire records and their controls. *Quaternary Science Reviews*, *65*, 5–25. https://doi.org/10.1016/j.quascirev.2012.11.029

McConnell, J. R., Edwards, R., Kok, G. L., Flanner, M. G., Zender, C. S., Saltzman, E. S., et al. (2007). 20th-century industrial black carbon emissions altered Arctic climate forcing. *Science*, *317*(5843), 1381–1384. https://doi.org/10.1126/science.1144856

Menon, S., Hansen, J., Nazarenko, L., & Luo, Y. (2002). Climate effects of black carbon aerosols in China and India. *Science*, *297*(5590), 2250–2253. https://doi.org/10.1126/science.1075159

Nghiem, S. V., Hall, D. K., Mote, T. L., Tedesco, M., Albert, M. R., Keegan, K., et al. (2012). The extreme melt across the Greenland ice sheet in 2012. *Geophysical Research Letters*, *39*, L20502. https://doi.org/10.1029/2012GL053611

Ocko, I. B., Ramaswamy, V., Ginoux, P., Ming, Y., & Horowitz, L. W. (2012). Sensitivity of scattering and absorbing aerosol direct radiative forcing to physical climate factors. *Journal of Geophysical Research*, *117*, D20203. https://doi.org/10.1029/2012JD018019

Oleson, K. W., Lawrence, D. M., Bonan, G. B., Flanner, M. G., Kluzek, E., Lawrence, P. J., et al. (2010). Technical description of version 4.0 of the Community Land Model (CLM), NCAR/TN-478+STR, National Center for Atmospheric Research, Boulder, CO.

Painter, T. H., Barrett, A. P., Landry, C. C., Neff, J. C., Cassidy, M. P., Lawrence, C. R., et al. (2007). Impact of disturbed desert soils on duration of mountain snow cover. *Geophysical Research Letters*, *34*, L12502. https://doi.org/10.1029/2007GL030284

Painter, T. H., Skiles, S. M., Deems, J. S., Bryant, A. C., & Landry, C. C. (2012). Dust radiative forcing in snow of the Upper Colorado River Basin: 1. A 6 year record of energy balance, radiation, and dust concentrations. *Water Resources Research*, *48*, W07521. https://doi.org/10.1029/2012WR011985

Polashenski, C. M., Dibb, J. E., Flanner, M. G., Chen, J. Y., Courville, Z. R., Lai, A. M., et al. (2015). Neither dust nor black carbon causing apparent albedo decline in Greenland's dry snow zone: Implications for MODIS C5 surface reflectance. *Geophysical Research Letters*, *42*, 9319–9327. https://doi.org/10.1002/2015GL065912

Ramanathan, V., & Carmichael, G. (2008, April). Global and regional climate changes due to black carbon. *Nature Geoscience*, *1*(4), 221–227. https://doi.org/10.1038/ngeo156

Sand, M., Berntsen, T. K., Kay, J. E., Lamarque, J.-F., Seland, Ø., & Kirkevåg, A. (2013). The Arctic response to remote and local forcing of black carbon. *Atmospheric Chemistry and Physics*, *13*(1), 211–224. https://doi.org/10.5194/acp-13-211-2013

Screen, J. A., Deser, C., & Simmonds, I. (2012). Local and remote controls on observed Arctic warming. *Geophysical Research Letters*, *39*, L10709. https://doi.org/10.1029/2012GL051598

Soja, A. J., Tchebakova, N. M., French, N. H. F., Flannigan, M. D., Shugart, H. H., Stocks, B. J., et al. (2007). Climate-induced boreal forest change: Predictions versus current observations. *Global and Planetary Change, Special NEESPI Issue*, *56*(3–4), 274–296. https://doi.org/10.1016/j.gloplacha.2006.07.028

Spracklen, D. V., Mickley, L. J., Logan, J. A., Hudman, R. C., Yevich, R., Flannigan, M. D., & Westerling, A. L. (2009). Impacts of climate change from 2000 to 2050 on wildfire activity and carbonaceous aerosol concentrations in the western United States. *Journal of Geophysical Research*, *114*, D20301. https://doi.org/10.1029/2008JD010966

Stocks, B. J., Fosberg, M. A., Lynham, T. J., Mearns, L., Wotton, B. M., Yang, Q., et al. (1998). Climate change and forest fire potential in Russian and Canadian boreal forests. *Climate Change*, *38*(1), 1–13. https://doi.org/10.1023/A:1005306001055

Stohl, A., Andrews, E., Burkhart, J. F., Forster, C., Herber, A., Hoch, S. W., et al. (2006). Pan-Arctic enhancements of light absorbing aerosol concentrations due to north American boreal forest fires during summer 2004. *Journal of Geophysical Research*, *111*, D22214. https://doi.org/10.1029/2006JD007216

Strellis, B. M., Bergin, M. H., Dibb, J. E., Sokolik, I., Sheridan, P., Orgen, J. A., et al. (2013). Aerosol radiative forcing over Central Greenland: Estimates based on field measurements, (Master's thesis). Retrieved from https://smartech.gatech.edu/bitstream/handle/1853/49063/STRELLIS-THESIS-2013.pdf

Thomas, J. L., Polashenski, C. M., Soja, A. J., Marelle, L., Casey, K., Choi, H. D., et al. (2017). Quantifying black carbon deposition over the Greenland ice sheet from forest fires in Canada. *Geophysical Research Letters*, *44*, 7965–7974. https://doi.org/10.1002/2017GL073701

Wang, C. (2004). A modeling study on the climate impacts of black carbon aerosols. *Journal of Geophysical Research*, *109*, D03106. https://doi.org/10.1029/2003JD004084

Wang, Q., Jacob, D. J., Fisher, J. A., Mao, J., Leibensperger, E. M., Carouge, C. C., et al. (2011). Sources of carbonaceous aerosols and deposited black carbon in the Arctic in winter-spring: Implications for radiative forcing. *Atmospheric Chemistry and Physics*, *11*(23), 12,453–12,473. https://doi.org/10.5194/acp-11-12453-2011

Wang, Y., Jiang, J. H., Su, H., Choi, Y.-S., Huang, L., Guo, J., & Yung, Y. L. (2018). Elucidating the role of anthropogenic aerosols in Arctic Sea ice variations. *Journal of Climate*, *31*(1), 99–114. https://doi.org/10.1175/JCLI-D-17-0287.1

Warren, S. G., & Wiscombe, W. J. (1980). A model for the spectral albedo of snow. II: Snow containing atmospheric aerosols. *Journal of the Atmospheric Sciences*, *37*, 2734–2745.